Avestia Publishing
International Journal of Theoretical and Applied Nanotechnology (IJTAN)
Volume 13, Year 2025
Journal ISSN: 1929-1248
DOI: 10.11159/ijtan.2025.001

Efficient CuO/ZnO/ZnAl Layered Double Hydroxide Photocatalyst for Methyl Orange Degradation

Zainab Hussaina Ibrahim[a,d], Zulkarnain Zainal[a.b], Lim Hong Ngee[a,b], Adila Mohamad Jaafar [a,c] and Mohd Haniff Wahid [a]

[a] Department of Chemistry, Faculty of Science, Universiti Putra Malaysia, 43400 Serdang, Selangor, Malaysia.
[b] Material Synthesis Laboratory, Institute of Advanced Technology, Universiti Putra Malaysia, 43400 Serdang, Selangor, Malaysia.
[c] Centre of Foundation Studies for Agricultural Science, Universiti Putra Malaysia, 43400 Serdang, Selangor, Malaysia.
zulkar@upm.edu.my, hongngee@upm.edu.my, adilamj@upm.edu.my, mw_haniff@upm.edu.my
[d] Department of Chemistry, Faculty of Science, Nigerian Defence Academy (NDA) Kaduna, PMB 2109, Nigeria.
zhibrahim@nda.edu.ng

Abstract- Dye-contaminated wastewater presents urgent environmental challenges requiring efficient treatment methods. This study reports a novel CuO/ZnO/ZnAl layered double hydroxide (LDH) photocatalyst synthesized via a one-pot modified co-precipitation and hydrothermal method optimized at 100 °C for 1 hour to preserve the LDH layered structure and enhance adsorption. Partial substitution of Zn^{2+} by 20 mol% Cu^{2+} formed CuO/ZnO heterojunctions, significantly improving light absorption by narrowing the bandgap from 3.06 to 2.46 eV and suppressing charge recombination. Under optimized conditions (0.125 g/L catalyst, 60 mg/L dye, pH 9), the catalyst achieved over 90% methyl orange degradation under both UV and visible light, with superoxide radicals as the dominant reactive species and excellent stability over three reuse cycles. These results demonstrate the synergistic effect of CuO and ZnO within the LDH matrix, providing a facile, effective approach for wastewater remediation through enhanced photocatalytic performance.

***Key Words*:** Layered double hydroxide, metal oxides, heterojunction, photodegradation, methyl orange.

Date Received: 2025-01-16
Date Revised: 2025-06-25
Date Accepted: 2025-08-28
Date Published: 2025-10-07

1. Introduction

The increasing demand for clean water has intensified research into sustainable nanomaterials[1] to remove persistent organic dyes from wastewater, such as methyl orange (MO), being a prevalent and challenging azo dye pollutant in industrial effluents [2]. Various treatment methods, including adsorption, membrane filtration, coagulation, advanced oxidation processes, microbial degradation, bio-electrochemical methods, and photocatalysis have been applied to address dye contamination [3-5]. Among these methods, photocatalysis stands out as a green and effective approach, utilizing semiconductor materials and solar energy to degrade pollutants under mild conditions [6].

Metal oxides such as ZnO and TiO_2 have been extensively studied for their photocatalytic capabilities [3], [7], [8], [9], owing to their ability to generate charge carriers upon light absorption that drive oxidation-reduction reactions [10]. However, their practical application is hindered by limitations including low surface area, rapid electron-hole recombination due to wide bandgap, and poor visible-light responsiveness [11]. To overcome these challenges, heterojunction photocatalysts integrating CuO with ZnO have been developed, extending light absorption into the visible spectrum and enhancing charge separation [7], [12].

Layered double hydroxides (LDHs) serve as effective hosts for metal oxides [13], offering high surface area, tunable compositions, anion exchange capacity, and environmental compatibility [14-16]. LDH nanomaterial possess a brucite-like layered structure expressed by the general formula $[M^{2+}_{1-x}M^{3+}_{x}(OH)_2](A^{n-})_{x/n}\cdot mH_2O]$, where M^{2+} and M^{3+} represent divalent and trivalent metal cations, respectively, and A^{n-} denotes charge-balancing interlayer anions [17]. The charge density of the layers, controlled by the molar ratio of M^{3+} to total metals, influences its structural and functional properties [18].

ZnAl layered double hydroxides (LDHs) exhibit photocatalytic activity under UV irradiation, primarily due to the formation of ZnO and $ZnAl_2O_4$ phases upon calcination [18], [19]. Incorporating Cu^{2+} into ZnAl LDH enables the synthesis of CuxO-containing LDHs, which extend light absorption into the visible region due to CuO's narrower bandgap and enhance charge separation efficiency [20], [21]. Despite these benefits, conventional synthesis methods often result in structural collapse caused by calcination above 450 °C, which declines adsorption performance [22], [23].

To address this, CuO/ZnO-based LDH heterojunctions have been developed to preserve the LDH layered framework while enhancing visible-light absorption and photocatalytic efficiency, offering a promising strategy for sustainable environmental remediation.

2. Related Works

Jiangfu Zheng et al. synthesized Cu_2O/ZnAl LDH composites through reconstitution of ZnAl layered double oxides with preformed Cu_2O nanoparticles, achieving visible-light-driven degradation of nitenpyram which demonstrate an I-scheme heterojunction mechanism [20]. Among their samples, 20% Cu_2O doping displayed superior performance. Eweis et al., employed a green synthesis technique to deposit CuO nanoparticles on ZnAl LDH templates, resulting in enhanced antimicrobial activity due to synergistic effects between CuO and the LDH support [24]. Zhang et al., reported an in-situ reduction method producing ultrathin Cu_2O on LDHs for visible light-driven nitrogen reduction [21], while Berede et al., developed biogenic CuO-decorated MgAl LDH catalysts that exhibited high surface area, uniform Cu distribution, and reduced electron-hole recombination, leading to improved methylene blue degradation [25].

These previous studies predominantly used reduction processes to deposit CuxO on LDHs, avoiding calcination to prevent structural damage. In contrast, calcination of Cu^{2+} containing LDH results in the formation of mixed metal oxides of $CuO/ZnO/Al_2O_3$ nanomaterial, mostly used in water-gas shift and steam reforming of methanol and ethanol [26], [27]. A major drawback is the low dispersion of CuO.

In this study, we report a modified co-precipitation synthesis of a CuO/ZnO/ZnAl LDH nanocomposite that preserves the LDH layered structure even after calcination, as confirmed by FTIR analysis showing characteristic carbonate (CO_3^{2-}) and hydroxide (OH^-) peak intensities. This nanocomposite exhibits superior adsorption capacity and efficient photocatalytic degradation of methyl orange under both UV and visible light due to efficient charge seperation, attributed to the synergistic effect of the CuO/ZnO heterojunction within the stable LDH framework.

3. Materials and Methodology

3.1 Materials

The chemicals used in this research are of analytical grade and were used without further purification. These include: zinc (II) nitrate hexahydrate (297.51 g/mol, 98 %) HmbG, copper (II) nitrate trihydrate (241.60 g/mol, assay > 99.0 %) Hayashi, aluminium (III) nitrate nonahydrate (375.13 g/mol, 98 %) Fluka, sodium hydroxide (40 g/mol, 99 %) R & M chemicals, ethanol (46.07 g/mol, assay > 99.9 %) Merck, EDTA disodium salt dihydrate (372.24 g/mol, assay > 99.0 %) BDH, ascorbic acid (176.13 g/mol, assay - 99.0 %) Fluka, UV light (9 W), halogen lamp (23 W) and cellulose nitrate filter (0.45 μm).

3.2 Methodology

A mixed aqueous solution of zinc nitrate $[Zn(NO_3)_2]$ and aluminum nitrate $[Al(NO_3)_3]$ salts, with a concentration of 0.4 M and a Zn:Al molar ratio of 4:1, was prepared as the precursor for synthesizing ZnO/ZnAl layered double hydroxide (LDH). Specifically, 2.375 g of $Zn(NO_3)_2$ and 0.75 g of $Al(NO_3)_3$ were dissolved in 25 mL of deionized water. The salt solution was co-precipitated by the simultaneous dropwise addition of 0.35 M sodium hydroxide (NaOH) solution and the metal ion solution into a reaction vessel containing 25 ml deionized water at 65 °C, under constant stirring, maintaining the pH at 10 throughout the reaction. After complete precipitation, the slurry was continuously stirred for an additional 1 hour to ensure full reaction and homogeneity.

Subsequently, the resulting mixture was subjected to hydrothermal treatment in a Teflon-lined stainless-

steel autoclave at an optimized temperature of 100 °C for 1 hour to enhance crystallinity and phase purity. The obtained solid product was then thoroughly washed with deionized water multiple times to remove residual ions, followed by drying at 65 °C until a constant mass was achieved. Finally, the dried material was calcined in air at 550 °C for 2 hours to obtain the desired ZnO/ZnAl LDH phase.

Using the same synthesis procedure, partial substitution of Zn^{2+} ions by Cu^{2+} ions was performed to prepare CuO/ZnO/ZnAl LDH samples with varying Cu loading levels from 5 to 30 mol%. The resulting samples were denoted as Cu-x LDH, where x represents the Cu content (5, 10, 20 and 30%).

The general reaction mechanism for the co-precipitation and hydrothermal synthesis can be represented as follows:

$$(4-\mathrm{x})\mathrm{Zn}^{2+} + \mathrm{xCu}^{2+} + Al^{3+} + OH^{-} \rightarrow CuO doped\ ZnO/\ ZnAl\ LDH \quad (1)$$

3.3 Photodegradation and Kinetics Study

Photodegradation of methyl orange (MO) was conducted using a 400 mL beaker containing 250 mL of MO solution at an initial concentration of 20 mg/L. The experiment was performed in a custom-fabricated closed reactor under stirring conditions to ensure homogeneity. Triplicate runs were conducted for each test, and the mean values are reported.

Approximately 0.005 g of the catalyst was dispersed into the MO solution and allowed for 30 minutes in the dark under stirring to establish adsorption-desorption equilibrium. Subsequently, the solution was exposed to ultraviolet (UV) light irradiation for 2 hours. The absorbance of MO was monitored at a wavelength of 463.1 nm using a UV-1100 spectrophotometer, and concentrations (C_t) were derived from a previously established calibration curve with a correlation coefficient (R^2) of 0.996.

The photodegradation efficiency was evaluated by plotting the relative concentration ratio (C_t/C_o) against time, where C_o is the initial MO concentration. Kinetic analysis was carried out by fitting the data to a pseudo-first-order kinetic model according to Eq. 2 below.

$$\ln\frac{C_o}{C_t} = \mathrm{k_{app}}t \quad (2)$$

Where k_{app} is the apparent rate constant (min^{-1}) and t is the irradiation time (minutes).

The effects of operational parameters on degradation performance were systematically investigated, including catalyst dosage (0.0125–0.125 g/L), initial dye concentration (20–60 mg/L), and solution pH (3–11).

3.4 Photocatalyst Evaluation

Reactive oxygen species (ROS) involvement in the photocatalytic process was assessed via scavenger tests under UV irradiation. Disodium EDTA, ascorbic acid, and ethanol were used to selectively quench; h^+ (holes), $\bullet O_2^-$ (superoxide radicals) and •OH (hydroxyl radicals) respectively [8].

Catalyst reusability and stability were examined over multiple cycles. After each cycle, the spent catalyst was recovered by filtration, washed thoroughly with deionized water, dried at 105 °C for 3 hours, and subsequently reused. Photodegradation performance during reuse was monitored by plotting C_t/C_o versus time for each cycle.

3.5 Characterization

Phase identification and crystallographic analysis were performed using X-ray diffraction (XRD) with a Philips PW 3040/60 diffractometer. The average crystallite size (D) was calculated using the Scherrer equation (Eq. 3), while the interlayer spacing (d) was determined from Bragg's law (Eq. 4):

$$\mathrm{D} = \frac{0.9\lambda}{\beta\cos\theta} \quad (3)$$

$$\mathrm{n}\lambda = 2\mathrm{d}\sin\theta \quad (4)$$

Where D is the average crystallite size (nm), K is the shape factor (typically 0.9), λ=0.154 nm is the wavelength of Cu K_α radiation, β is the full width at half-maximum (FWHM) of the diffraction peak (in radians), θ is the Bragg angle in degrees, and n is the order of reflection (n = 1).

Fourier-transform infrared (FTIR) spectroscopy was conducted using a Perkin Elmer Spectrum 100 to identify functional groups present in the samples. Optical properties, specifically the absorption edge, were analyzed by UV-Visible diffuse reflectance spectroscopy (UV-DRS) using a Shimadzu UV-3600 spectrometer and the bandgap energy (Eg) values were calculated via Tauc plots following Eq. 5:

$$(\alpha h\upsilon)^{\mathrm{n}} = \mathrm{B}(h\upsilon - \mathrm{E_g}) \quad (5)$$

Where α is the absorption coefficient, h is Planck's constant, ν is the incident photon frequency, B is the proportionality constant, and n=2 for direct allowed transitions.

Morphological investigations were performed via field emission scanning electron microscopy (FESEM, JEOL JSM 7600F) coupled with energy-dispersive X-ray spectroscopy (EDX) mapping for elemental distribution, the atomic weight percentage was calculated via Eq. 6. Surface area and porosity characteristics, including specific surface area and pore size distribution, were examined using Brunauer-Emmett-Teller (BET) and Barrett-Joyner-Halenda (BJH) methods with a TriStar II Plus surface analyzer.

$$Atomic\ weight\ (\%_i) = \frac{\omega_i/A_i}{\sum_v \omega_v/A_v} \times 100 \quad (6)$$

Where ω_i is weight % of a given metal and A_i its corresponding atomic mass. ω_v and A_v are the total weight percent and atomic masses of the elements.

4. Results and Discussion

4.1 Optimization of Synthesis Conditions for MO Degradation

The synthesis of ZnO/ZnAl LDH was systematically optimized by varying two key hydrothermal parameters: temperature (100, 120, and 150 °C) and holding time (1 to 3 hours). The results demonstrated that lower hydrothermal temperatures significantly enhanced the degradation efficiency of methyl orange (MO), with the optimal performance achieved at 100 °C. This trend is illustrated in Figure 2a, where the catalytic degradation of MO was most efficient under this condition. Similarly, shorter hydrothermal holding times correlated with higher degradation rates as seen in Figure 2b, indicating that prolonged treatment may adversely affect catalytic activity.

This enhancement at lower temperatures and shorter durations can be attributed to the better preservation of the layered double hydroxide (LDH) structure. The preserved LDH framework facilitates stronger interactions between intercalated anions (CO_3^{2-} and OH^-) and dye molecules during the photocatalytic process [3], [28] thereby improving adsorption and subsequent degradation efficiency. This effect aligns with literature reports on the crucial role of LDH structural integrity in photocatalytic applications [20], [25].

Figure 2c presents a comprehensive comparison of the photocatalytic abilities of ZnO/ZnAl LDH catalysts with varying Cu^{2+} substitution (5–30 %). A distinct relationship emerges between Cu content and degradation efficiency.

Notably, all samples exhibit some adsorption in the dark. The Cu-5 and Cu-10 LDH samples show greater dark adsorption, suggesting more accessible active sites or stronger surface interaction with MO. The sample containing Cu-20, demonstrates the least adsorption and highest MO degradation efficiency, achieving about 60% removal after UV light exposure, using 0.02 g/L of the catalyst. This improved performance is attributed to an optimal balance in adsorption in the pre-irradiation phase and heterojunction formation, which likely facilitates efficient charge carrier separation and minimizes recombination, as supported by previous heterojunction studies [29]. Increasing the Cu content to 30 % resulted in a drop in the degradation efficiency. This suggests that excessive Cu incorporation may cause structural disruption or introduce defects that hinder charge transfer, lowering catalytic performance.

Figure 2d shows the corresponding pseudo-first-order kinetic analysis for the degradation of MO using Cu-substituted samples. The fastest rate constant was depicted by Cu-20 LDH ($0.0052 min^{-1}$), followed by Cu-10 LDH ($0.0029 min^{-1}$) and progressively slower rates for Cu-5 and 30 % content ($0.002 min^{-1}$). The linearity of the plots and corresponding rate constants confirm superior kinetics at moderate doping, while high Cu levels diminish activity.

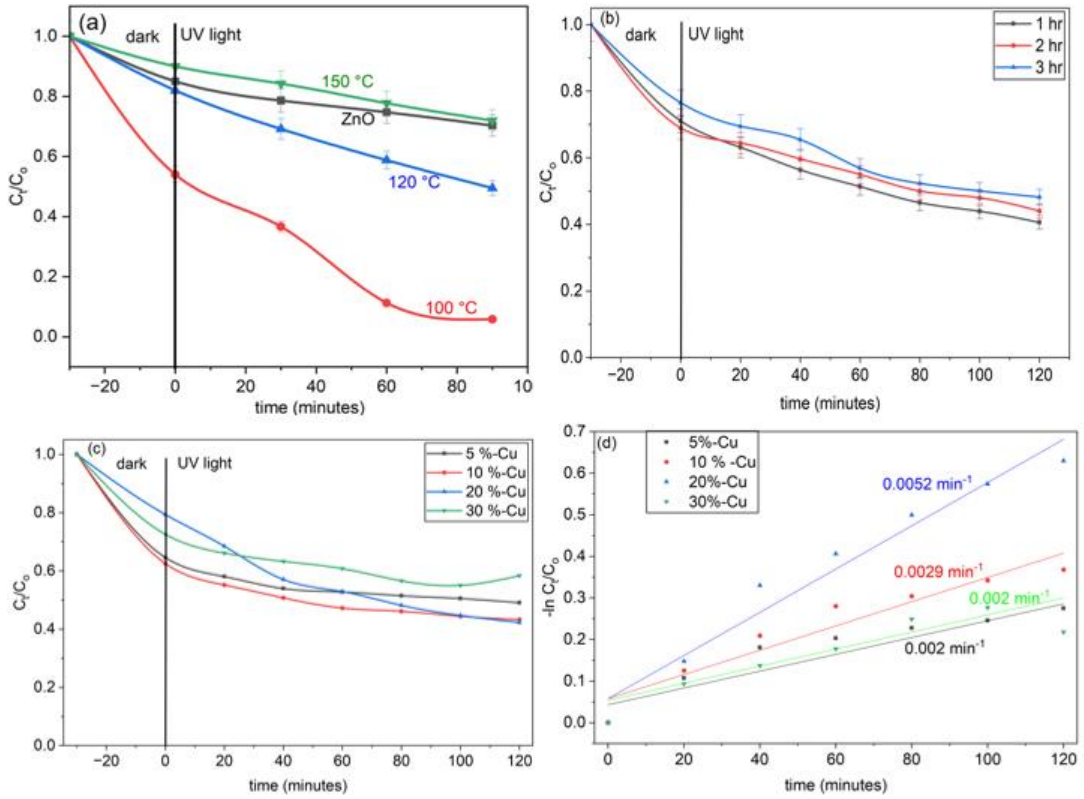

Figure 2: Effect of varying hydrothermal conditions on MO degradation; (a) temperature (0.05 g/L in 20 mg/L MO), (b) holding time (0.02 g/L in 20 mg/L MO), : (c) effect of Cu-substituted ZnO/ZnAl LDH on the degradation of MO (0.02 g/L, 20 mg/L MO) and (d) corresponding degradation kinetics.

4.2 Optimization of Parameters and Kinetics Study

The effect of varying experimental conditions on the degradation of MO using Cu-20 LDH is depicted in Figures 3. Increasing the catalyst dose proportionately enhances degradation efficiency by supplying more reactive surface area for adsorption as shown in Figure 3a, conversely, higher MO concentrations (Figure 3b) lead to decreased degradation efficiency, likely due to active site saturation and light attenuation effects. Under optimized conditions (0.125g/L of catalyst and 60mg/L MO), the pH-dependence of the Cu-20 LDH is elucidated in Figure 3c. Optimum MO removal is observed at pH 9 with over 60 % adsorption, attaining 88 % degradation after 30 minutes of UV light irradiation, underscoring the significance of alkaline conditions for surface charge and pollutant-catalyst interactions. The catalyst maintains high activity from pH 3–9, but performance drops beyond pH 9, attributed to increased competition between MO and excess hydroxide ions (OH^-) for adsorption sites [30].

Figure 3d highlights the superiority of Cu-20 LDH in both UV and visible light photodegradation at optimized conditions (0.125g/L, 60mg/L and pH 9). It shows the kinetic analysis via apparent rate constants which confirms enhanced catalytic activity, with Cu-20 LDH yielding a rate constant of 0.021min^{-1} (R^2=0.9571) under UV light and 0.018 min^{-1} (R^2=0.9883) under visible light irradiation. This demonstrates the capacity for effective visible-light activation, highlighting its

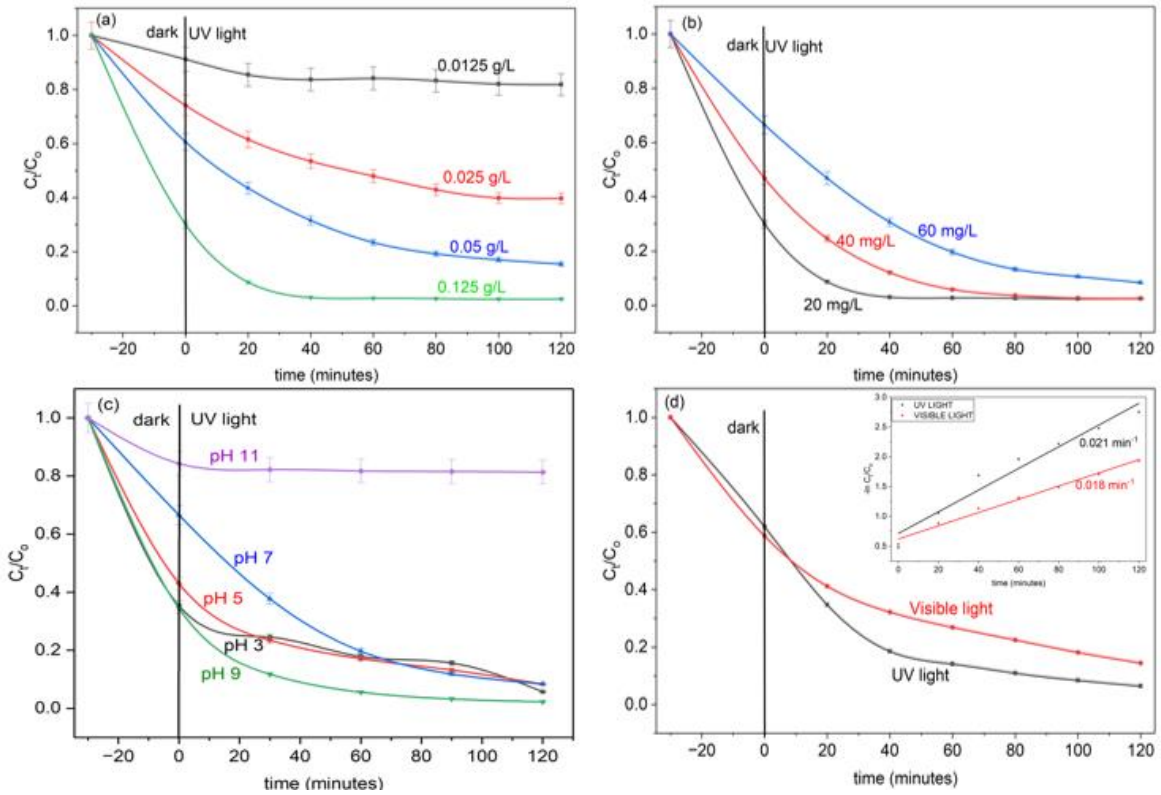

Figure 3: Effect of varying parameters on the degradation of MO using Cu-20 LDH; (a) catalyst dose (20 mg/L MO, pH 7), (b) MO concentration (0.125 g/L, pH 7), (c) varying pH (0.125 g/L and 60 mg/L MO) and (d) varying light source (0.125 g/L, 60 mg/L MO and pH 9).

potential for solar-driven photocatalytic applications in wastewater treatment.

4.3 Photocatalyst Evaluation

Superoxide radicals ($\bullet O_2^-$) played the dominant role in MO dye degradation as illustrated in Figure 4a, which is confirmed by the pronounced reduction in photocatalytic activity upon quenching with ascorbic acid. The reactive species contribution followed the order: $\bullet O_2^- > h^+ > \bullet OH$.

The catalyst's reusability, assessed over three consecutive cycles (Figure 4b), retained over 80 % degradation efficiency, indicating excellent stability. This durability is likely due to the suppression of photo-corrosion [31] through efficient charge carrier separation during photocatalysis [29].

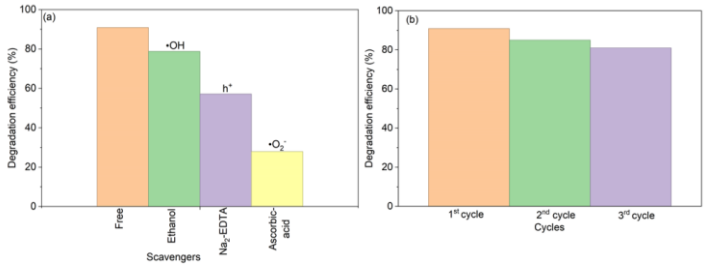

Figure 4: Effect of scavenging radicals on MO degradation (a) and reusability test (b), using Cu-20 LDH

4.4 Characterization of Photocatalyst

Figure 5a displays the PXRD patterns of commercial ZnO as a reference sample and the synthesized ZnO/ZnAl LDH samples synthesized at

different hydrothermal temperatures after calcination. The diffraction peaks indexed at 2θ values of approximately 11.6°, 23.3°, and 34.49° correspond to the (003), (006), and (012) planes characteristic of the LDH phase [24], [32]. Additionally, prominent ZnO reflections at 31.88°, 34.65°, and 36.64° confirm the coexistence of ZnO within the ZnO/ZnAl LDH heterostructure, indicating a successful synthesis [14], [33], [34]. Notably, despite calcination at a relatively high temperature of 550 °C, partial preservation of the LDH crystal structure

synthesized at 100 °C exhibits superior photocatalytic degradation of methyl orange (MO), attributed to the synergistic combination of a well-defined ZnAl LDH framework and ZnO nanoparticles. This heterostructure benefits from the high surface area of the LDH matrix and the photocatalytic activity of ZnO. Consequently, the facile hydrothermal synthesis at 100 °C effectively preserves both ZnAl LDH and ZnO phases, establishing it as the optimal synthesis condition for achieving enhanced photocatalytic performance.

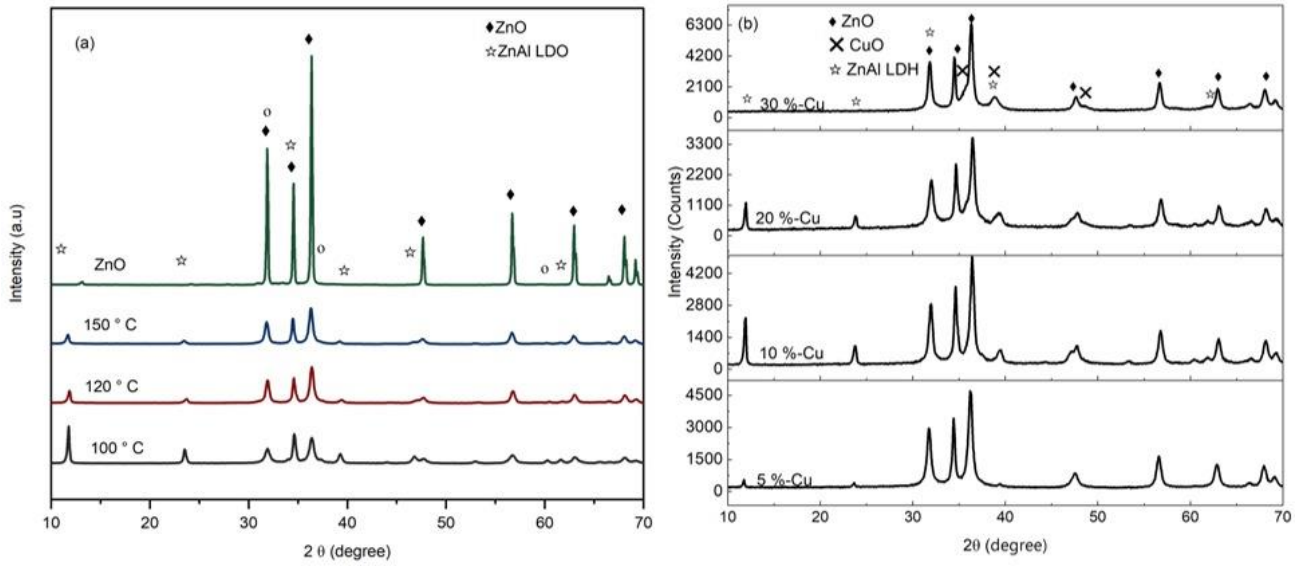

Figure 5: PXRD plots of: ZnO/ZnAl LDH at varying hydrothermal temperatures (a) and Cu-substituted ZnO/ZnAl LDH (b)

was observed. This behaviour deviates from the typical LDH thermal decomposition threshold near 300 °C [22], suggesting enhanced thermal stability in this system. Such structural retention likely plays a critical role in maintaining active sites essential for adsorption of pollutants, potentially contributing to improved catalytic efficiency [23], [31].

Increasing the hydrothermal temperature from 100 °C to 150 °C led to a significant decrease in the intensity of LDH-related peaks alongside an increase in ZnO peak intensity. This trend implies reduced LDH crystallinity and partial transformation of the ZnAl LDH phase into ZnO. Rietveld refinement quantitatively proved this phase evolution, revealing an increase in ZnO content from 62.7% to 86.4% with hydrothermal temperature from 100 °C to 150 °C respectively, accompanied by a concomitant decline in the LDH phase and associated interlayer anions, as evident from the attenuation of LDH-specific reflections. Earlier degradation test has demonstrated that ZnO/ZnAl LDH

The PXRD patterns of Cu-substituted ZnO/ZnAl LDH (Figure 5b) confirm the formation of CuO, in addition to ZnO and ZnAl LDH heterostructures, evidenced by distinct diffraction peaks corresponding to each phase. With 10 % Cu content, new reflection peaks at 2θ positions 36°, 38° and 48° begin to emerge, which are characteristics of CuO [35]. Phase composition, quantified via Rietveld refinement are summarized in Table 1, which indicates the retention of the LDH structure with low Cu incorporation.

The Rietveld refinement reveals a systematic increase of the CuO phase fraction with CuO content 0.1, 14.1, 21.4 and 27.7 % for 5, 10, 20, 30% Cu, respectively, accompanied by a non-monotonic evolution of ZnO; 7.3, 70.1, 69.2 and 72.3 %, while the LDH phase peaks at 10 % Cu content before declining at 20 % Cu and becoming negligible at 30 % Cu content. These trends indicate that average Cu incorporation promotes intimate CuO nucleation on ZnO/ZnAl LDH surfaces while higher contents favour phase segregation into standalone CuO

and ZnO domains [12]. The lattice parameters a and d_{110} remain constant across 5 – 20 % Cu content, indicating a stable metal–metal spacing, while the c parameter which indicates the thickness of the film, confirms carbonate-intercalated LDHs. The basal spacing (003) shows a slight contraction from 7.54 to 7.42 Å, for 5 to 20 % Cu, which we ascribe to tighter interlayer binding with increasing Cu content, consistent with literature [36]. The crystallite size varies non-monotonically. These results are consistent with literature attributing improved photocatalytic performance to built-in fields at the CuO/ZnO interface [37, 38].

Table 1: Rietveld Refinement Composition of Heterostructure ZnO/ZnAl LDH Varying Cu Content.

Crystallographic Parameters	Amount of Cu-doping (%)			
	5	10	20	30
a (Å)[a]	3.076	3.076	3.076	-
c (Å)[a]	22.809	22.809	22.809	-
$\mathbf{c^1}$ (Å)[a] (interlayer thickness)	7.603	7.603	7.603	-
d_{110} (a/2) [a]	1.538	1.538	1.538	-
D (nm)	12.21	15.41	11.36	15.36
Basal spacing (003) reflection [a]	7.54	7.45	7.42	-
ZnO phase (%)	97.3	70.1	69.2	72.3
CuO phase (%)	0.1	14.1	21.4	27.7
LDH phase (%)	2.3	15.8	9.3	-

[a] LDH

To study the optical properties of Cu-substituted LDHs, UV-Vis diffuse reflectance spectra were obtained. The spectra (Figure 6a) exhibit a progressive red shift in absorption edge with increasing Cu^{2+} content (5-30%), indicative of bandgap narrowing. The presence of M^{II}-O-M^{III} band structure within the LDH may induce new energy levels, which can reduce the band gap energy and consequently enhance visible light response of the material [39]. As shown in Figure 6b the bandgap decreased from 3.01 eV to 2.4 eV, thereby enhancing the material's response to visible light. The Photocatalytic performance evaluation identified Cu-20 LDH as the most efficient sample, achieving the highest degradation efficiency, mainly due to its retained LDH structure and proper heterostructure between the components. Hence, further characterization focused exclusively on Cu-20 LDH composition.

FTIR spectra (Figure 6c) of ZnO/ZnAl LDH and Cu-20 LDH reveal peaks corresponding to interlayer species; hydroxyl groups and carbonate anions (OH^- and CO_3^{2-}) [40], with diminished intensity in the Cu-20 LDH, consistent with a retained stacked LDH structure. It is worth noting that ZnAl Layer Double Oxides (LDO) only reveal metal oxide vibration peaks [5] resulting from the loss of water molecules and interlayer anions.

BET surface area analysis of Cu-20 LDH shows a typical type IV isotherm with H3-type hysteresis loops (Figure 6d), confirming the presence of mesopores structure. The measured surface area and average pore diameter were 47.35 m^2/g and 8.2 nm, respectively. These textural properties are characteristic of lamellar LDH structures and contribute to the material's high adsorption capacity.

The extent of separation of photogenerated charge carriers was investigated using the photoluminescence spectra (PL) of ZnO/ZnAl LDH and Cu-20 LDH. The PL spectra is depicted in Figure 6e, with an excitation wavelength of 320 nm, a broad emission in ZnO/ZnAl LDH was observed which is indicative of many recombination channels. Peaks at 390 – 420 nm can be ascribed to band-to-band recombination in ZnO [32] while peaks around 440 – 520 nm are due to defect-related emissions, from oxygen vacancies or surface states. This reveals that the ZnO/ZnAl layered double hydroxide (LDH) exhibits significantly high electron-hole recombination. In contrast, Cu-20 LDH shows a suppressed PL emission, indicating more efficient charge separation. The reduction in recombination observed in the Cu-20 LDH material can be attributed to the formation of a p-n heterojunction by CuO and ZnO, which facilitates directional charge transfer of electrons from CuO to ZnO to ZnAl LDH, while holes in the opposite direction [14], [41]. This directional charge transfer minimizes radiative recombination losses, thereby promoting the overall photocatalytic efficiency and narrowing the bandgap slightly, which improves visible-light absorption.

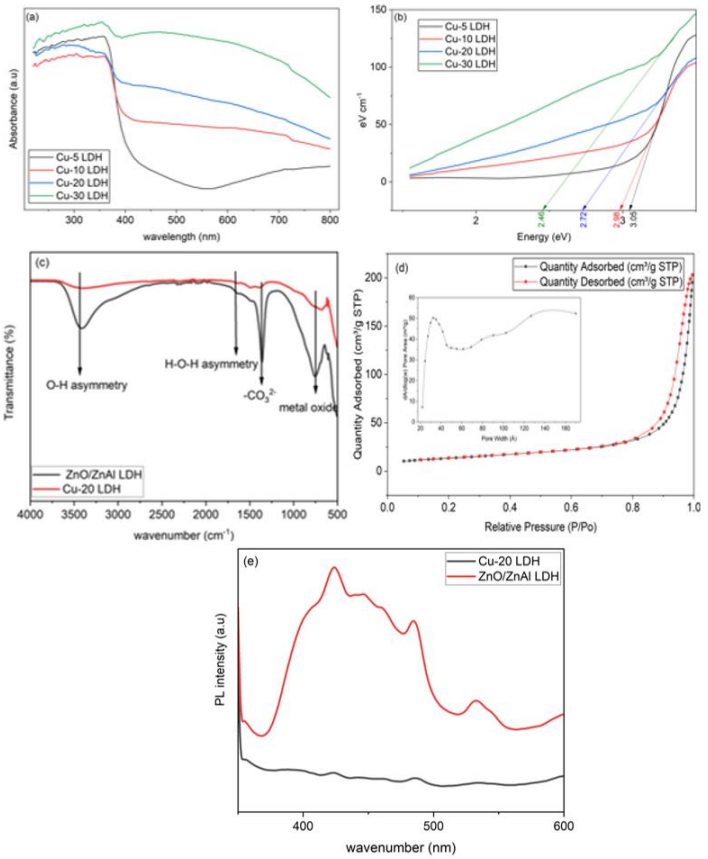

Figure 6: UV-DRS plots of Cu-substituted ZnO/ZnAl LDH (a), corresponding bandgap energies (b), FTIR plot (c), Nitrogen adsorption-desorption isothermal plots (pore size distribution- inset) (d) and photoluminescence spectrum of Cu-20 LDH.

The FESEM images of as synthesized ZnO/Zn−Al LDH and Cu-20 LDH are revealed in Figures 7a and b respectively, having distorted hexagonal plate-like morphology in a lamellar structure, which is characteristic of LDH materials [24] in the presence of smaller metal oxide nanoparticles. The images reveal an average lateral sizes of 27.5 and 13.4 nm for ZnO/ZnAl LDH and Cu-20 LDH respectively, while the corresponding elemental mapping of Cu-20 LDH (Figure 7c) confirms a uniform distribution of composition, which is characteristic of LDH [42].

The presence of C and O in the elemental analysis confirm the existence of CO_3^{2-} and OH^- intercalation in the Cu-20 LDH, which depict the stability of the material having undergone calcination at 550 °C. EDX analysis of the Cu-20 LDH sample (surface-sensitive) revealed Cu, Zn and Al weight percent of 10.97, 47.84, and 3.09 wt% respectively. The corresponding metals atomic percentages, calculated from Eq. 6, yields 16.94, 71.82 and 11.24 for Cu, Zn and Al respectively.

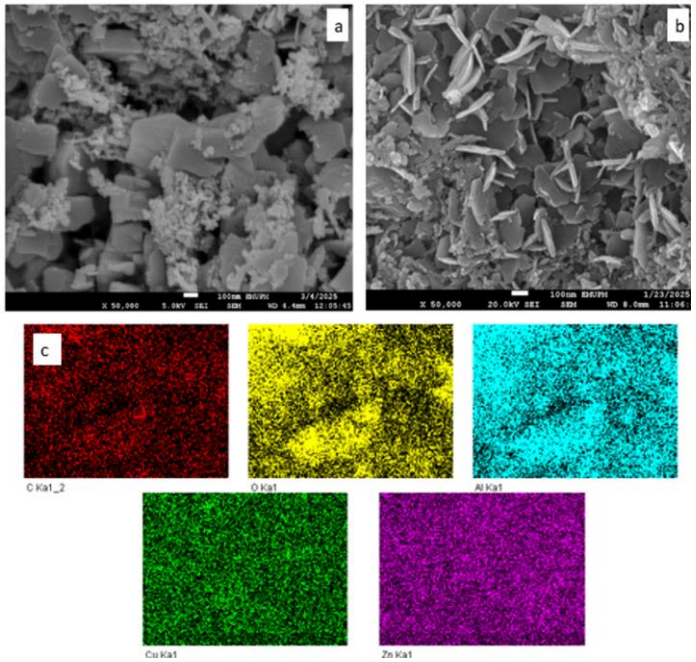

Figure 7: FESEM images of ZnO/ZnAl LDH (a) Cu-20 LDH (b) and corresponding elemental mapping of Cu-20 LDH (c).

The Cu fraction within the divalent sublattice, Cu/(Cu+Zn) = 19.1%, closely matches the nominal 20% substitution target. However, the divalent: trivalent ratio inferred from EDX gives an approximately 7.9:1, which deviates from the synthesis target (4:1). This may be attributed to surface enrichment of Al-free ZnO/CuO phases, limited Al detection by EDX, and carbon support contributions.

Table 2: Elemental weight percent of Cu-20 LDH from EDX analysis.

Elements	Weight Percent (%)
Cu	10.97
Zn	47.84
Al	3.09
C	25.36
O	12.74

The proposed photocatalytic mechanism for MO degradation using Cu-20 LDH is depicted in Eqs. 7 – 10, derived from the heterostructure's band alignment and ROS evaluation, is illustrated as follows. Upon light irradiation, CuO/ZnO/ZnAl LDH absorbs photons energy, promoting electrons from the valence band (VB)

to the conduction band (CB) of each component, thereby generating e^- – h^+ pairs. Owing to the heterostructure's favourable band offsets and high electrical conductivity, photogenerated electrons preferentially migrate to the CB of ZnAl LDH, while holes accumulate in the VB of CuO (Eq. 6), facilitating efficient charge separation.

The transferred electrons react with dissolved O_2 to yield superoxide radicals ($\bullet O_2^-$) (Eq. 6), whereas holes oxidize surface-bound water to produce hydroxyl radicals (•OH) (Eq. 7) [43]. The synergistic action of •OH, $\bullet O_2^-$, and h^+ enhance the mineralizes MO into CO_2 and H_2O (Eq. 8 -10).

$$CuO/ZnO/ZnAl + h\upsilon \rightarrow CuO(h^+) + ZnAl(e^-) \quad (5)$$

$$ZnAl\ (e^-) + O_{2\ (ads)} \rightarrow CuO/ZnO/ZnAl(e^-) + \bullet O_2^- \quad (6)$$

$$CuO\ (h^+) + H_2O \rightarrow CuO/ZnO/ZnAl(h^+) + H^+ + \bullet OH \quad (7)$$

$$\bullet O_2^- + MO \rightarrow \text{degradation products} \quad \text{(fast)} \quad (8)$$

$$\bullet OH + MO \rightarrow \text{degradation products} \quad (9)$$

$$h^+ + MO \rightarrow \text{degradation products} \quad (10)$$

Table 3 presents a comparative investigation of different CuO/ZnO composites used as photocatalyst for pollutant degradation and their corresponding efficiencies.

Conclusion

In conclusion, a heterojunction nano-catalyst was generated within the layered double hydroxide matrix, the nano-catalyst CuO/ZnO/ZnAl LDH benefited from characteristics of the layered structure of ZnAl LDH and heterojunction of CuO/ZnO enhancing the adsorption and photodegradation properties respectively. CuO (p-type) in contact with ZnO (n-type) forms p–n junctions that enhance charge separation and visible light response, with an optimal Cu loading of 20 %, Cu maximizes junction density for charge separation, consistent with literature linking improved photocatalytic performance to built-in fields at the CuO/ZnO interface. A preliminary study revealed the nanomaterials' exceptional photodegradation capacity for the model pollutant methyl orange, depicting the materials potential to be used for environmental remediation.

Nevertheless, the present work is limited to a model pollutant under controlled conditions, and long-term stability, recyclability, and performance in real wastewater systems remain to be investigated. Future studies should focus on scaling up the synthesis, exploring broader classes of organic and inorganic contaminants, and employing in-situ characterization or computational modeling to gain deeper mechanistic insight. Such directions will be essential to translate the promising laboratory performance of CuO/ZnO/ZnAl

Table 3: Summary of various CuO/ZnO composite for pollutant degradation.

CuO/ZnO Composite	Pollutant(s)	Parameters	Degradation Efficiency	References
Cu2O/ZnAl-LDH	Nitenpyram	20 mg/100 mL, 10 mg L^{-1}	99%	[20]
p-n CuO/ZnO	Methyl orange	8 g /L, 5 mg/L, pH 4	91%	[38]
ZnO/CuO n-n heterojunction	Acid Orange 7	0.1 g L^{-1}, 5 mg L^{-1}	80.5%	[44]
CuO@ZnO NPs	Methylene Blue	30 mg/50 mL, 5 ppm	98%	[3]
ZnO/CuO/GO	Rhodamine Blue	35 mg/50 mL, 10 mg/L	99%	[45]
ZnO/CuO/rGO	Rhodamine Blue and 4-chlorophenol	0.1 g/100 mL, 5 ppm and pH 11	99% and 93%	[46]
Cu2O/CuZnAl-LDHs)	Tetracycline	5 mg /100 mL 50 mg/L	94.1%	[23]
CuO/ZnO/ZnAl (LDH)	Methyl orange	0.125 g/L, 60 mg/L, and pH 9	90 %	This work

LDH heterojunctions into practical water treatment technologies.

Acknowledgement

We wish to acknowledge the financial support of Geran Putra GP – IPS/2023/9746900, which was used for the research analyses, and RSC Researcher Development and Travel Grant (D24-1663108605) for conference.

References

[1] A. Singh, A. Mittal, and N. K. Jangid, "Toxicology of Dyes," in *Impact of Textile Dyes on Public Health and the Environment*, IGI Global Scientific Publishing, 2020, pp. 50–69. doi: 10.4018/978-1-7998-0311-9.ch003.

[2] A. Pandey, V. M. Pathak, Navneet, and M. Rajput, "A feasible approach for azo-dye (methyl orange) degradation by textile effluent isolate Serratia marcescens ED1 strain for water sustainability: AST identification, degradation optimization and pathway hypothesis," *Heliyon*, vol. 10, no. 11, p. e32339, June 2024, doi: 10.1016/j.heliyon.2024.e32339.

[3] P. Nepal, S. Parajuli, G. P. Awasthi, K. P. Sharma, H. B. Oli, R. L. Shrestha, and D. P. Bhattarai "Eco-Friendly Synthesis of CuO@ZnO Nanocomposites Using Artemisia vulgaris Leaf Extract and Study of Its Photocatalytic Activity for Methylene Blue," *Journal of Nanotechnology*, vol. 2024, no. 1, p. 6896986, 2024, doi: 10.1155/2024/6896986.

[4] T. Shindhal, *P* Rakholiya, S. Varjani, A. Pandey, H. H.Ngo, W. Guo, H. Y. Ng and M. T. Taher. "A critical review on advances in the practices and perspectives for the treatment of dye industry wastewater," *Bioengineered*, vol. 12, no. 1, pp. 70–87, Jan. 2021, doi: 10.1080/21655979.2020.1863034.

[5] Rohmatullaili, N. Ahmad, D. Erviana, Zultriana, D. Savira, R. Mohadi and A. Lesbani "Enhancing the performance of modified ZnAl LDH as hybrid catalyst-adsorbent on tetracycline removal under solar light irradiation," *Inorganic Chemistry Communications*, vol. 161, p. 112101, Mar. 2024, doi: 10.1016/j.inoche.2024.112101.

[6] M. Xiao, Z. Wang, M. Lyu, B. Luo, S. Wang, G. Liu, H. Cheng, and L. Wang. "Hollow Nanostructures for Photocatalysis: Advantages and Challenges," *Advanced Materials*, vol. 31, no. 38, p. 1801369, 2019, doi: 10.1002/adma.201801369.

[7] M. Jeevarathinam and I. V. Asharani, "Synthesis of CuO, ZnO nanoparticles, and CuO-ZnO nanocomposite for enhanced photocatalytic degradation of Rhodamine B: a comparative study," *Sci Rep*, vol. 14, no. 1, p. 9718, Apr. 2024, doi: 10.1038/s41598-024-60008-7.

[8] M. L. J. Peerlings, K. Han, A. Longo, K. H. Helfferich, M. Ghiasi, P. E. de Jongh, and P. Ngene. "Synthesis and Catalytic Performance of Bimetallic Oxide-Derived CuO–ZnO Electrocatalysts for CO2 Reduction," *ACS Catal.*, vol. 14, no. 14, pp. 10701–10711, July 2024, doi: 10.1021/acscatal.4c01575.

[9] M. Nasrollahzadeh, M. Sajjadi, S. Iravani, and R. S. Varma, "Green-synthesized nanocatalysts and nanomaterials for water treatment: Current challenges and future perspectives," *Journal of Hazardous Materials*, vol. 401, p. 123401, Jan. 2021, doi: 10.1016/j.jhazmat.2020.123401.

[10] X. Yu, Y. Hu, C. Shao, W. Huang, and Y. Li, "Polymer semiconductors: A unique platform for photocatalytic hydrogen peroxide production," *Materials Today*, vol. 71, pp. 152–173, Dec. 2023, doi: 10.1016/j.mattod.2023.10.005.

[11] M. J. Wu, J.Z. Wu, J. Zhang, H. Chen, J.Z. Zhou, G.R. Qian, Z. P. Xu, Z. Du and Q.L. Rao "A review on fabricating heterostructures from layered double hydroxides for enhanced photocatalytic activities," *Catal. Sci. Technol.*, vol. 8, no. 5, pp. 1207–1228, Mar. 2018, doi: 10.1039/C7CY02314F.

[12] A. G. Bekru, L. T. Tufa, O. A. Zelekew, M. Goddati, J. Lee, and F. K. Sabir, "Green Synthesis of a CuO–ZnO Nanocomposite for Efficient Photodegradation of Methylene Blue and Reduction of 4-Nitrophenol," *ACS Omega*, vol. 7, no. 35, pp. 30908–30919, Sept. 2022, doi: 10.1021/acsomega.2c02687.

[13] R. Sharma, G. G. C. Arizaga, A. K. Saini, and P. Shandilya, "Layered double hydroxide as multifunctional materials for environmental remediation: from chemical pollutants to microorganisms," *Sustainable Materials and Technologies*, vol. 29, p. e00319, Sept. 2021, doi: 10.1016/j.susmat.2021.e00319.

[14] H. Tang, X. Luo, W. Li, Y Pan, S. Wang, H. Ma, Y Shen, R. Fang and F. Dong "Highly active Ag/ZnO/ZnAl-LDH heterojunction photocatalysts for NO removal," *Chemical Engineering Journal*, vol. 474, p. 145873, Oct. 2023, doi: 10.1016/j.cej.2023.145873.

[15] D. L. Gao, W. W. Lin, Q. J. Lin, F. F. Dai, Y. X. Xue, J. H. Chen, Y. X. Liu, Y. Huang, Q. Yang. "Remarkable

adsorption capacity of Cu2+-doped ZnAl layered double hydroxides and the calcined materials toward phosphate," *Journal of Environmental Chemical Engineering*, vol. 11, no. 2, p. 109472, Apr. 2023, doi: 10.1016/j.jece.2023.109472.

[16] B. Benalioua, M. Mansour, A. Bentouami, B. Boury, and E. H. Elandaloussi, "The layered double hydroxide route to Bi–Zn co-doped TiO2 with high photocatalytic activity under visible light," *Journal of Hazardous Materials*, vol. 288, pp. 158–167, May 2015, doi: 10.1016/j.jhazmat.2015.02.013.

[17] M. Nocchetti, M. Pica, B. Ridolfi, A. Donnadio, E. Boccalon, G. Zampini, D. Pietrella and M. Casciola. "AgCl-ZnAl Layered Double Hydroxides as Catalysts with Enhanced Photodegradation and Antibacterial Activities," *Inorganics*, vol. 7, no. 10, Art. no. 10, Oct. 2019, doi: 10.3390/inorganics7100120.

[18] H. Asghar, V. Maurino, and M. A. Iqbal, "Development of Highly Photoactive Mixed Metal Oxide (MMO) Based on The Thermal Decomposition Of ZnAl-NO3-LDH," Mar. 08, 2024, *Chemistry and Materials Science*. doi: 10.20944/preprints202403.0534.v1.

[19] E. M. Seftel, M. Niarchos, Ch. Mitropoulos, M. Mertens, E. F. Vansant, and P. Cool, "Photocatalytic removal of phenol and methylene-blue in aqueous media using TiO2@LDH clay nanocomposites," *Catalysis Today*, vol. 252, pp. 120–127, Sept. 2015, doi: 10.1016/j.cattod.2014.10.030.

[20] J. Zheng, C. Fan, X. Li, Q. Yang, D. Wang, A. Duan and S. Pan "Efficient mineralisation and disinfection of neonicotinoid pesticides with unique ZnAl-LDH intercalation structure and synergistic effect of Cu2O crystalline surface," *Colloids and Surfaces A: Physicochemical and Engineering Aspects*, vol. 687, p. 133507, Apr. 2024, doi: 10.1016/j.colsurfa.2024.133507.

[21] S. Zhang, Y. Zhao, R. Shi, C. Zhou, G. I. N. Waterhouse, Z. Wang, Y. Weng and T. Zhang "Sub-3 nm Ultrafine Cu2O for Visible Light Driven Nitrogen Fixation," *Angewandte Chemie International Edition*, vol. 60, no. 5, pp. 2554–2560, 2021, doi: 10.1002/anie.202013594.

[22] S.-B. Lee, E.-H. Ko, J. Y. Park, and J.-M. Oh, "Mixed Metal Oxide by Calcination of Layered Double Hydroxide: Parameters Affecting Specific Surface Area," *Nanomaterials*, vol. 11, no. 5, Art. no. 5, May 2021, doi: 10.3390/nano11051153.

[23] X. Ran, T. Sun, R. Zhou, C. Wei, W. Gao, and H. Zhao, "*In situ* formation of Cu_2 O decorated CuZnAl-layered double hydroxide heterostructured photocatalysts for enhancing the degradation of tetracycline under visible light," *New J. Chem.*, vol. 47, no. 6, pp. 2914–2923, 2023, doi: 10.1039/D2NJ04564H.

[24] A. A. Eweis, M. S. Ahmad, E. B. El Domany, M. Al-Zharani, M. Mubarak, Z. E Eldin, Y. GadelHak, R. Mahmoud, and W. N. Hozzein. "Actinobacterium-Mediated Green Synthesis of CuO/Zn–Al LDH Nanocomposite Using *Micromonospora* sp. ISP-2 27: A Synergistic Study that Enhances Antimicrobial Activity," *ACS Omega*, vol. 9, no. 32, pp. 34507–34529, Aug. 2024, doi: 10.1021/acsomega.4c02133.

[25] H. T. Berede, D. M. Andoshe, N. S. Gultom, D. Kuo, X. Chen, H. Abdullah, T. H. Wondimu, Y. Wu and O. A. Zelekew "Photocatalytic activity of the biogenic mediated green synthesized CuO nanoparticles confined into MgAl LDH matrix," *Sci Rep*, vol. 14, no. 1, p. 2314, Jan. 2024, doi: 10.1038/s41598-024-52547-w.

[26] S. Kühl, M. Friedrich, M. Armbrüster, and M. Behrens, "Cu,Zn,Al layered double hydroxides as precursors for copper catalysts in methanol steam reforming – pH-controlled synthesis by microemulsion technique," *J. Mater. Chem.*, vol. 22, no. 19, pp. 9632–9638, Apr. 2012, doi: 10.1039/C2JM16138A.

[27] D. Li, S. Xu, Y. Cai, C. Chen, Y. Zhan, and L. Jiang, "Characterization and Catalytic Performance of Cu/ZnO/Al2O3 Water–Gas Shift Catalysts Derived from Cu–Zn–Al Layered Double Hydroxides," *Ind. Eng. Chem. Res.*, vol. 56, no. 12, pp. 3175–3183, Mar. 2017, doi: 10.1021/acs.iecr.6b04337.

[28] M. Singh, S. Bhadauria, and S. Meena, "Physico-Chemical Analysis of Textile Effluents from Bagru, Jaipur (Rajasthan, India): Implications for Environmental Impact and Treatment Needs," *Asian Journal of Environment & Ecology*, vol. 23, no. 11, pp. 118–130, Nov. 2024, doi: 10.9734/ajee/2024/v23i11627.

[29] R. Yang, W. Mu, L. He, J. Meng, X. Bi, W. Luo, S. Luo and X. Lei "CdS/NiCoAl-LDH heterojunction for superior photocatalytic hydrogen production and stability in water splitting," *Chemical Engineering Journal*, vol. 503, p. 158495, Jan. 2025, doi: 10.1016/j.cej.2024.158495.

[30] S. Li, S. Yan, Z. Tong, X. Yong, X. Zhang, and J. Zhou, "Assessment of photocatalytic activities of layered double hydroxide@petrochemical sludge biochar for sulfamethoxazole degradation," *Separation and Purification Technology*, vol. 355, p. 129732, Mar. 2025, doi: 10.1016/j.seppur.2024.129732.

[31] A. Balapure, J. R. Dutta, and R. Ganesan, "Recent advances in semiconductor heterojunctions: a detailed review of the fundamentals of photocatalysis, charge transfer mechanism and materials," *RSC Applied Interfaces*, vol. 1, no. 1, pp. 43–69, 2024, doi: 10.1039/D3LF00126A.

[32] D. Peng, Q. Jing, Z. Feng, J. Niu, X. Cheng, X. Wu, X. Zheng and X. Yuan "Facile preparation of AB-stacking graphene oxide/ZnAl-layered double hydroxide composites and enhanced visible-light photocatalytic performance of the calcined product," *Journal of Physics and Chemistry of Solids*, vol. 136, p. 109199, Jan. 2020, doi: 10.1016/j.jpcs.2019.109199.

[33] L. Smoláková, L. Dubnová, J .Kocík, J. Endres, S. Daniš, P. Priecel and L. Čapek "*In-situ* characterization of the thermal treatment of Zn-Al hydrotalcites with respect to the formation of Zn/Al mixed oxide active in aldol condensation of furfural," *Applied Clay Science*, vol. 157, pp. 8–18, June 2018, doi: 10.1016/j.clay.2018.02.024.

[34] Y. Wang, H. Li, J. Xu, J. Yu, J. Wang, H. Jiang, C. Li, X. Zhang and N. Liu. "High-performance carbon@ metal oxide nanocomposites derived metal–organic framework-perovskite hybrid boosted microwave-induced catalytic degradation of norfloxacin: Performance, degradation pathway and mechanism," *Separation and Purification Technology*, vol. 330, p. 125399, Feb. 2024, doi: 10.1016/j.seppur.2023.125399.

[35] M. Răciulete, G. Layrac, D. Tichit, and I.-C. Marcu, "Comparison of CuxZnAlO mixed oxide catalysts derived from multicationic and hybrid LDH precursors for methane total oxidation," *Applied Catalysis A: General*, vol. 477, pp. 195–204, May 2014, doi: 10.1016/j.apcata.2014.03.018.

[36] Bhojaraj, C. Nethravathi, and M. Rajamathi, "Intercalation and separation of isomeric nitrophenols using the anionic clay, Mg2Al(OH)6(CO3)0.5·nH2O and the structurally related layered hydroxy salt, Ni3Zn2(OH)8(CH3COO)2·mH2O," *Applied Clay Science*, vol. 243, p. 107053, Oct. 2023, doi: 10.1016/j.clay.2023.107053.

[37] S. P. Murzin, "Formation of ZnO/CuO Heterostructures Based on Quasi-One-Dimensional Nanomaterials," *Applied Sciences*, vol. 13, no. 1, p. 488, Jan. 2023, doi: 10.3390/app13010488.

[38] N. T. T. Vo, S.-J. You, M.-T. Pham, and V. V. Pham, "A green synthesis approach of p-n CuO/ZnO junctions for multifunctional photocatalysis towards the degradation of contaminants," *Environmental Technology & Innovation*, vol. 32, p. 103285, Nov. 2023, doi: 10.1016/j.eti.2023.103285.

[39] M. S. Seyed Dorraji, M. H. Rasoulifard, H. Daneshvar, A. Vafa, and A. R. Amani-Ghadim, "ZnS/ZnNiAl-LDH/GO nanocomposite as a visible-light photocatalyst: preparation, characterization and modeling," *J Mater Sci: Mater Electron*, vol. 30, no. 13, pp. 12152–12162, July 2019, doi: 10.1007/s10854-019-01573-w.

[40] B. Nagendra, C. V. S. Rosely, A. Leuteritz, U. Reuter, and E. B. Gowd, "Polypropylene/Layered Double Hydroxide Nanocomposites: Influence of LDH Intralayer Metal Constituents on the Properties of Polypropylene," *ACS Omega*, vol. 2, no. 1, pp. 20–31, Jan. 2017, doi: 10.1021/acsomega.6b00485.

[41] A. Janotti and C. G. Van de Walle, "Fundamentals of zinc oxide as a semiconductor," *Rep. Prog. Phys.*, vol. 72, no. 12, p. 126501, Oct. 2009, doi: 10.1088/0034-4885/72/12/126501.

[42] M. Chafiq, A. Chaouiki, R. Salghi, and Y. G. Ko, "Fabrication of branch-like Aph@LDH-MgO material through organic-inorganic hybrid conjugation for excellent anti-corrosion performance," *Journal of Magnesium and Alloys*, vol. 11, no. 7, pp. 2469–2485, July 2023, doi: 10.1016/j.jma.2023.06.002.

[43] S. Girish Kumar and K. S. R. Koteswara Rao, "Zinc oxide based photocatalysis: tailoring surface-bulk structure and related interfacial charge carrier dynamics for better environmental applications," *RSC Advances*, vol. 5, no. 5, pp. 3306–3351, 2015, doi: 10.1039/C4RA13299H.

[44] S. Ruan, W. Huang, M. Zhao, H. Song, and Z. Gao, "A Z-scheme mechanism of the novel ZnO/CuO n-n heterojunction for photocatalytic degradation of Acid Orange 7," *Materials Science in Semiconductor Processing*, vol. 107, p. 104835, Mar. 2020, doi: 10.1016/j.mssp.2019.104835.

[45] H. Long, R. Huang, X. Liu, and C. Chen, "Preparation and photocatalytic performance of ZnO/CuO/GO heterojunction under visible light," *Inorganic*

Chemistry Communications, vol. 136, p. 109097, Feb. 2022, doi: 10.1016/j.inoche.2021.109097.

[46] H. Li, W. Ma, X. Zeng, S. Liu, L. Xiao, Z. Fang, Y. Feng, M. Yang, H. Zhu, Y. Yang and H. Liu. "ZnO/CuO Piezoelectric Nanocatalysts for the Degradation of Organic Pollutants," *ACS Appl. Nano Mater.*, vol. 6, no. 22, pp. 21113–21122, Nov. 2023, doi: 10.1021/acsanm.3c04168.